IEEE Robotics and Automation Letters (RAL) paper presented at
2024 IEEE/RSJ International Conference on Intelligent Robots and Systems (IROS)
October 14-18, 2024. Abu Dhabi, UAE

Contact Representation in Robotic Mechanical Systems Employing Reduced Models

Ali Raoofian, Xu Dai, and József Kövecses

***Abstract*—Contact interactions play a major role in the dynamic analysis of robotic arms, where they can be represented as unilateral constraints. However, incorporating these contacts into the system dynamic model is a challenging task, given the numerous ways to account for them. This letter presents and compares two different approaches to contact modelling, highlighting how adopting a different perspective can avoid constraint redundancies and indeterminate problems. To this end, a co-simulation setup is employed as the primary framework to address the differences in the contact modelling approaches and the corresponding formulations. In a co-simulation setup, a system is divided into subsystems that exchange information at pre-determined communication points through the interface. Between the communication time points, the subsystems are integrated independently while they require updated interface variables from other subsystems. Hence, it is necessary to approximate these variables. In a model-based approximation, a reduced model of the subsystem emulates its dynamic behaviour at the interface. This letter addresses challenges in developing a representative reduced order model for a mechanical subsystem with contacts and proposes solutions to incorporate changes in contact states in the reduced model. It will be shown how basic assumptions in the contact dynamic incorporation can influence the simulation outcome. To demonstrate the proposed solution, a robotic arm model and its operations are used as a case study.**

***Index Terms*—Co-simulation, model order reduction, dynamic simulation, non-smooth system, contact modelling, constraint redundancy.**

I. Introduction

ROBOTIC systems are becoming more and more physically/mechanically diverse. Simulation plays an increasingly important role in the design, control, and interaction of such systems. In a complex mechanical system it is not always feasible to represent all elements of the system in a monolithic formulation. Including additional capabilities to an existing modelling, such as contact representation, comes with redesigning and development costs. Co-simulation can provide an alternative solution in such cases, where the different elements can be modelled separately and coupled/interfaced in a co-simulation setup.

In a co-simulation setup, subsystems exchange data at discrete time points termed *communication points*. The time interval between them is the *macro time step*. Simulation of each subsystem is then carried out independently using different integration methods and step sizes, also known as *micro time steps*. As subsystems are interfaced with each other, the interface variables should be determined during the macro time-step integration. Some methods compute these variables through iteration [1]. In real-time applications, restarting the subsystem time stepping from a previous state is not possible. Hence, in such applications, non-iterative co-simulation schemes are used where, the subsystems exchange required data at each communication point and continue with their time stepping independently until end of the macro time step. Thus, the interface variables need to be approximated during the macro time step. There are two main approaches for the prediction of interface variables, namely, *signal-based* and *model-based* methods. Signal-based approaches rely on extrapolation from past history of the interface variables without accounting for the physical nature of the subsystem. Such methods range from zero-order hold method to higher degree polynomials [2] and smoothing techniques [4].

Benefits of the signal-based techniques are limited in real-time simulations [5] as the macro step size controls the stability. Model-based coupling methods can have significant advantages over signal-based techniques in functionality, simulation stability and accuracy of the results [6]. In such methods, a *reduced order model* of the subsystem will be developed that turns the complex multibody system model into a simpler low-dimensional model. This reduced model gives an accurate representation of the dynamics that is necessary for the interfacing in the macro time step. Such a model is known as *reduced interface model* (RIM). The concept of RIM was first introduced in [7] for systems with smooth dynamic behaviour. Then, the concept was extended to non-smooth mechanical systems with unilateral interactions [5].

The introduction of a RIM in the co-simulation leads to the scheme shown in Fig. 1. Here, we describe the model-based co-simulation for two mechanical subsystems of a robotic arm. However, this can be generalized to multiple subsystems. Consider a mechanical system partitioned into two subsystems that interact with each other through the interface in between. Here, we consider a multirate setup where the two subsystems use different integration time step sizes h_1 and h_2. As shown

Manuscript received 4 August 2023; accepted 5 December 2023. Date of publication 13 December 2023; date of current version 8 January 2024. This letter was recommended for publication by Associate Editor Marco Costanzo and Editor Hong Liu upon evaluation of the reviewers' comments. This work was supported by the Natural Sciences and Engineering Research Council of Canada (NSERC) and CM Labs Simulations Inc. Ali Raoofian was also supported by the Fonds de Recherche du Québec– Nature et Technologies (FRQNT), Canada. *(Corresponding author: Ali Raoofian.)*

The authors are with the Department of Mechanical Engineering and Centre for Intelligent Machines, McGill University, Montréal, QC H3A 0C3, Canada (e-mail: ali.raoofian@mail.mcgill.ca; xu.dai@mail.mcgill.ca; jozsef.kovecses@mcgill.ca).

Digital Object Identifier 10.1109/LRA.2023.3342549

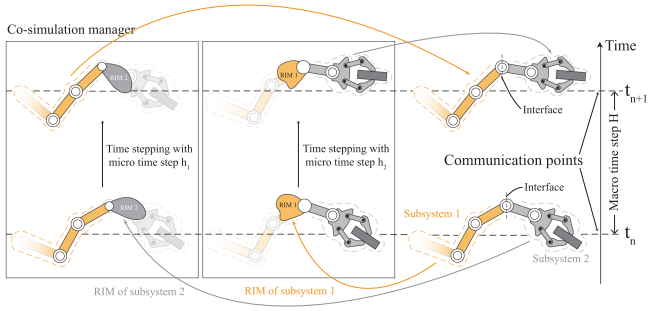

(a) Time stepping of two subsystems in one macro time step.

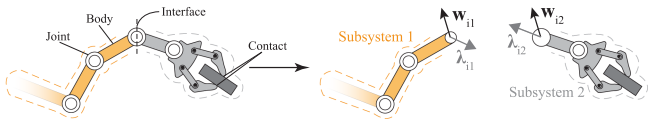

(b) The subsystems and their generalized interface velocity and force arrays.

Fig. 1. Model-based co-simulation of mechanical systems using reduced interface models (RIMs).

in the figure, at each communication point, the RIM of each mechanical subsystem is generated and sent to the co-simulation manager. Then, each subsystem is time stepped with a specified micro time step together with the RIM of the other subsystem. The time stepping continues until the end of the macro time step H. Then, the full model of each subsystem is captured. The interface definition together with the corresponding velocities and forces are shown in Fig. 1(b).

Constructing a RIM for non-smooth systems is a complex task and some challenges need to be addressed. The state of the unilateral interactions in such systems can change to "open" or "closed" due to the attachment/detachment of the contact points. Consequently, these contact state changes should also be taken into account in the model-reduction phase. One way to develop the reduced model is to assume that the most recent state of the contacts captured at the communication point will remain unchanged during the macro time step. This is the main idea behind the RIM development in [5], [8]. Such an assumption can give promising results extending from simple planar models [5] to large-scale systems like, robotics-astronaut training simulators [3], [8]. This reduced model is known as *smooth-RIM* because it treats the closed contact points as bilateral constraints during the macro step and the resulting reduced model is basically a smooth system.

Such smooth RIMs can have good performance in many cases but, they may not be representative enough in certain situations as was shown in [6]. In this letter, the smooth and the non-smooth RIMs are described and applied to a large-scale robot arm that undergoes a contact task. It will be shown that the non-smooth-RIM would allow for including the contact state transition inside the macro time step by keeping the important complementarity conditions of the contacts in the RIM formulations.

II. Non-Smooth Mechanical System Dynamics

Consider a mechanical subsystem interfaced with other subsystems and subjected to bilateral constraints and unilateral interactions (e.g. subsystem 2 in Fig. 1). The configuration and the velocity of a mechanical system can be parameterized with a set of n_q generalized coordinates $\mathbf{q}$ and n generalized velocities $\mathbf{v}$ which are related by transformation $\dot{\mathbf{q}} = \mathbf{N}\mathbf{v}$, where $\mathbf{N}(\mathbf{q})$ is the $n_q \times n$ transformation matrix; in general $n_q \geq n$. In this system, the general constraints at the velocity level can be formulated by a set of m_c constraint velocity components $\mathbf{w}_c = [w_1 \quad w_2 \quad \dots \quad w_{m_c}]^T$ as

$$\mathbf{w}_c = \mathbf{A}_c \mathbf{v} \tag{1}$$

where $\mathbf{A}_c(\mathbf{q})$ is the $m_c \times n$ constraint Jacobian matrix. If the constraints are holonomic then they may also be represented at the configuration level as $\mathbf{\Phi}(\mathbf{q}, t) = \mathbf{0}$ or $\mathbf{\Phi}(\mathbf{q}, t) \geq \mathbf{0}$ such that $\dot{\mathbf{\Phi}} = \mathbf{A}_c \mathbf{v} + \partial \mathbf{\Phi}/\partial t$ where $\mathbf{w}_c = -\partial \mathbf{\Phi}/\partial t$. Likewise, the $m_i \times 1$ interface velocity of a mechanical subsystem $\mathbf{w}_i$ can be mapped from the generalized velocity array $\mathbf{v}$ as:

$$\mathbf{w}_i = \mathbf{A}_i \mathbf{v} \tag{2}$$

where $\mathbf{A}_i$ is a $m_i \times n$ Jacobian matrix corresponding to the interface velocity that characterizes the dynamics of the mechanical subsystem at the interface. The dynamic equations of this subsystem can be written as

$$\mathbf{M}\dot{\mathbf{v}} + \mathbf{c} = \mathbf{f}_o + \mathbf{A}_c^T \boldsymbol{\lambda}_c + \mathbf{A}_i^T \boldsymbol{\lambda}_i \tag{3}$$

where $\mathbf{M}(\mathbf{q})$ is the $n \times n$ mass matrix, $\mathbf{c}(\mathbf{q}, \mathbf{v})$ is the $n \times 1$ array of Coriolis and centrifugal terms, $\mathbf{f}_o$ is the $n \times 1$ array of generalized applied forces. $\boldsymbol{\lambda}_c$ and $\boldsymbol{\lambda}_i$ are the $m_c \times 1$ and $m_i \times 1$ array of constraint interaction forces and interface forces, respectively. Note that $\boldsymbol{\lambda}$ is a generalized force since it can contain either force or moment elements depending on the constrained or interface velocity in the corresponding $\mathbf{w}$.

A. Unilateral Constraints and Complementarity Problem

By including the constraint acceleration $\dot{\mathbf{w}}_c$, the dynamic and kinematic equations together can be written as

$$\begin{bmatrix} \mathbf{M} & -\mathbf{A}_c^T \\ \mathbf{A}_c & \mathbf{0} \end{bmatrix} \begin{bmatrix} \dot{\mathbf{v}} \\ \boldsymbol{\lambda}_c \end{bmatrix} = \begin{bmatrix} \mathbf{f}_o - \mathbf{c} + \mathbf{A}_i^T \boldsymbol{\lambda}_i \\ \dot{\mathbf{w}}_c - \dot{\mathbf{A}}_c \mathbf{v} \end{bmatrix} \tag{4}$$

For now, it is assumed that $\boldsymbol{\lambda}_i$ is a known value. In practice, (4) should be solved together with the dynamic equations of the other subsystem for the interface and $\boldsymbol{\lambda}_i$ would be determined that way. In a general case, the constraints of the system can be grouped into *bilateral* and *unilateral* ones, i.e., $\mathbf{w}_c = [\mathbf{w}_b^T \quad \mathbf{w}_u^T]^T$. Unilateral constraints can be used, for example, to model *contact* interactions in a system model. When there are closed contacts in the system model, complementarity conditions [9] are introduced and the representation of the unilateral constraints can be formulated as [10]

$$\mathbf{0} \leq \dot{\mathbf{w}}_u \perp \boldsymbol{\lambda}_u \geq \mathbf{0} \tag{5}$$

where $\boldsymbol{\lambda}_u$ is the normal contact force, $\dot{\mathbf{w}}_u$ is the contact acceleration and $\perp$ represents the component-wise complementarity between the elements of acceleration and force, i.e., $\lambda_{uj} \dot{w}_{uj} = 0, \forall j$. The constraint formulation in (5) makes sure that the contact force is zero when a contact opens, and allows only for a positive force value in case of a closed contact.

In a more general form, the dynamic equations with the constraints form a mixed linear complementarity problem

(MLCP) [11]

$$\begin{cases} \begin{bmatrix} \mathbf{M} & -\mathbf{A}_{\mathrm{b}}^{\mathrm{T}} & -\mathbf{A}_{\mathrm{u}}^{\mathrm{T}} \\ \mathbf{A}_{\mathrm{b}} & \mathbf{0} & \mathbf{0} \\ \mathbf{A}_{\mathrm{u}} & \mathbf{0} & \mathbf{0} \end{bmatrix} \begin{bmatrix} \dot{\mathbf{v}} \\ \boldsymbol{\lambda}_{\mathrm{b}} \\ \boldsymbol{\lambda}_{\mathrm{u}} \end{bmatrix} + \begin{bmatrix} \mathbf{c} - \mathbf{f}_{\mathrm{o}} - \mathbf{A}_{\mathrm{i}}^{\mathrm{T}} \boldsymbol{\lambda}_{\mathrm{i}} \\ \dot{\mathbf{A}}_{\mathrm{b}} \mathbf{v} \\ \dot{\mathbf{A}}_{\mathrm{u}} \mathbf{v} \end{bmatrix} = \begin{bmatrix} \mathbf{0} \\ \dot{\mathbf{w}}_{\mathrm{b}} \\ \dot{\mathbf{w}}_{\mathrm{u}} \end{bmatrix} \\ \mathbf{0} \leq \dot{\mathbf{w}}_{\mathrm{u}} \perp \boldsymbol{\lambda}_{\mathrm{u}} \geq \mathbf{0} \end{cases} \tag{6}$$

In order to solve this problem, first the contact forces should be determined. To this end, one can calculate $\dot{\mathbf{v}}$ and $\boldsymbol{\lambda}_{\mathrm{b}}$ from the first two rows and substitute them into the third row. This will turn the problem into a standard linear complementarity problem (LCP) as

$$\begin{cases} \mathbf{L}\boldsymbol{\lambda}_{\mathrm{u}} + \mathbf{b} = \dot{\mathbf{w}}_{\mathrm{u}} \\ \mathbf{0} \leq \dot{\mathbf{w}}_{\mathrm{u}} \perp \boldsymbol{\lambda}_{\mathrm{u}} \geq \mathbf{0} \end{cases} \tag{7}$$

where $\mathbf{L}$ is the lead matrix and $\mathbf{b}$ is the array of remaining terms:

$$\mathbf{L} = \begin{bmatrix} \mathbf{A}_{\mathrm{u}} & \mathbf{0} \end{bmatrix} \begin{bmatrix} \mathbf{M} & -\mathbf{A}_{\mathrm{b}}^{\mathrm{T}} \\ \mathbf{A}_{\mathrm{b}} & \mathbf{0} \end{bmatrix}^{-1} \begin{bmatrix} \mathbf{A}_{\mathrm{u}}^{\mathrm{T}} \\ \mathbf{0} \end{bmatrix}$$

$$\mathbf{b} = \begin{bmatrix} \mathbf{A}_{\mathrm{u}} & \mathbf{0} \end{bmatrix} \begin{bmatrix} \mathbf{M} & -\mathbf{A}_{\mathrm{b}}^{\mathrm{T}} \\ \mathbf{A}_{\mathrm{b}} & \mathbf{0} \end{bmatrix}^{-1} \begin{bmatrix} \mathbf{c} - \mathbf{f}_{\mathrm{o}} - \mathbf{A}_{\mathrm{i}}^{\mathrm{T}} \boldsymbol{\lambda}_{\mathrm{i}} \\ -\dot{\mathbf{A}}_{\mathrm{b}} \mathbf{v} \end{bmatrix} + \dot{\mathbf{A}}_{\mathrm{u}} \mathbf{v}$$

The LCP in (7) can be solved in different ways, for example using direct pivoting methods or iterative techniques. Once the values of $\lambda_{\mathrm{u}j}$ and $\dot{w}_{\mathrm{u}j}$ are found, the unilateral interactions can be categorized into *active* and *tight* sets. The active set is referred to the closed contact pairs. The associated active contact forces in $\boldsymbol{\lambda}_{\mathrm{a}}$ have non-negative values, i.e., $\lambda_{\mathrm{a}j} \in [0, +\infty)$ and according to the complementarity condition, $\dot{\mathbf{w}}_{\mathrm{a}} = \mathbf{0}$. For the tight set, the corresponding contact forces and accelerations are represented by $\boldsymbol{\lambda}_{\mathrm{t}} = \mathbf{0}$ and $\dot{w}_{\mathrm{t}j} \in [0, +\infty)$, respectively. The categorization after solving the LCP can be shown as

$$\boldsymbol{\lambda}_{\mathrm{u}} = \begin{bmatrix} \boldsymbol{\lambda}_{\mathrm{a}} \\ \boldsymbol{\lambda}_{\mathrm{t}} \end{bmatrix}, \quad \dot{\mathbf{w}}_{\mathrm{u}} = \begin{bmatrix} \dot{\mathbf{w}}_{\mathrm{a}} \\ \dot{\mathbf{w}}_{\mathrm{t}} \end{bmatrix} = \begin{bmatrix} \mathbf{A}_{\mathrm{a}} \dot{\mathbf{v}} + \dot{\mathbf{A}}_{\mathrm{a}} \mathbf{v} \\ \mathbf{A}_{\mathrm{t}} \dot{\mathbf{v}} + \dot{\mathbf{A}}_{\mathrm{t}} \mathbf{v} \end{bmatrix} \tag{8}$$

Once the state of the contacts is known, we can return to (6) and solve the dynamic equations to time step the system to the next time point.

III. Reduced Order Model Formulations

In order to develop a reduced model of any mechanical subsystem as a part of a larger system, first, we need to take a second look at the unilateral interactions within that subsystem. The reduced model is always developed based on information at the communication points. Thus, the most recent state of the contacts are known. We can regroup the constraint velocities of the subsystem and their corresponding Jacobians as below

$$\mathbf{w}_{\mathrm{c}} = \begin{bmatrix} \mathbf{w}_{\mathrm{b}} \\ \mathbf{w}_{\mathrm{u}} \end{bmatrix} = \begin{bmatrix} \mathbf{w}_{\mathrm{b}} \\ \mathbf{w}_{\mathrm{a}} \\ \mathbf{w}_{\mathrm{t}} \\ \mathbf{w}_{\mathrm{p}} \end{bmatrix} = \begin{bmatrix} \mathbf{w}_{\alpha} \\ \mathbf{w}_{\mathrm{t}} \\ \mathbf{w}_{\mathrm{p}} \end{bmatrix} = \begin{bmatrix} \mathbf{A}_{\alpha} \\ \mathbf{A}_{\mathrm{t}} \\ \mathbf{A}_{\mathrm{p}} \end{bmatrix} \mathbf{v} \tag{9}$$

We group the constraints into three subgroups. The *active*, *tight* and *potential* constraints. A group of contacts that are active and will remain active until the next communication point, such as bilateral constraints, are shown with subscript 'a' and their constraint velocity is $\mathbf{w}_{\mathrm{a}}$. Similarly, $\mathbf{w}_{\mathrm{t}}$ can be defined for the tight contacts. However, a new group of *potential* contacts are defined here that are prone to change state, e.g., active contacts that might open during the macro step. Their corresponding velocity and Jacobian are shown with $\mathbf{w}_{\mathrm{p}}$ and $\mathbf{A}_{\mathrm{p}}$, respectively. Finally, we gather the bilateral and active unilateral constraints together as the new set of active constraints, i.e., $\mathbf{w}_{\alpha} = [\mathbf{w}_{\mathrm{b}}^{\mathrm{T}} \quad \mathbf{w}_{\mathrm{a}}^{\mathrm{T}}]^{\mathrm{T}}$, and show them with subscript 'α'. The potential contacts are kept in complementarity form. With such a re-grouping, the dynamic formulation (3) can be rewritten as

$$\begin{cases} \mathbf{M}\dot{\mathbf{v}} + \mathbf{c} = \mathbf{f}_{\mathrm{o}} + \mathbf{A}_{\mathrm{i}}^{\mathrm{T}} \boldsymbol{\lambda}_{\mathrm{i}} + \mathbf{A}_{\alpha}^{\mathrm{T}} \boldsymbol{\lambda}_{\alpha} + \mathbf{A}_{\mathrm{t}}^{\mathrm{T}} \boldsymbol{\lambda}_{\mathrm{t}} + \mathbf{A}_{\mathrm{p}}^{\mathrm{T}} \boldsymbol{\lambda}_{\mathrm{p}} \\ \mathbf{0} \leq \dot{\mathbf{w}}_{\mathrm{p}} \perp \boldsymbol{\lambda}_{\mathrm{p}} \geq \mathbf{0} \end{cases} \tag{10}$$

A. Decoupling Dynamic Equations in a Sub-Space of Interest

From the geometric point of view, the configuration of a mechanical system can be viewed as a configuration space and the related Euclidean tangent space $\mathcal{V}$. The velocity of a mechanical system can be represented as a vector in this tangent space, $\mathbf{v} \in \mathcal{V}$ [12]. It is always possible to select a sub-space $\mathcal{S} \subseteq \mathcal{V}$ with parameterization of generalized velocity $\mathbf{w}_{\mathcal{S}} \in \mathcal{S}$ [12]. The subspace that complements the space $\mathcal{S}$ is also shown with $\mathcal{A}$, where $\mathcal{S} \cup \mathcal{A} \equiv \mathcal{V}$ and $\mathbf{w}_{\mathcal{A}} \in \mathcal{A}$. The transformation between the parameterization of these spaces can be shown as

$$\begin{bmatrix} \mathbf{A}_{\mathcal{S}} \\ \mathbf{A}_{\mathcal{A}} \end{bmatrix} \mathbf{v} = \begin{bmatrix} \mathbf{w}_{\mathcal{S}} \\ \mathbf{w}_{\mathcal{A}} \end{bmatrix} = \mathbf{w} \tag{11}$$

The above transformation is always valid for any sub-space $\mathcal{S}$ as long as the elements of the arrays are independent, i.e., $\mathbf{w}$ forms an alternative, full parameterization for the tangent space $\mathcal{V}$. If $\mathbf{M}_{\mathrm{v}}$ and $\mathbf{M}_{\mathrm{w}}$ represent the mass matrices associated with parametrizations $\mathbf{v}$ and $\mathbf{w}$, it can be shown that [12]

$$\mathbf{M}_{\mathrm{w}}^{-1} = \begin{bmatrix} \mathbf{A}_{\mathcal{S}} \mathbf{M}_{\mathrm{v}}^{-1} \mathbf{A}_{\mathcal{S}}^{\mathrm{T}} & \mathbf{A}_{\mathcal{S}} \mathbf{M}_{\mathrm{v}}^{-1} \mathbf{A}_{\mathcal{A}}^{\mathrm{T}} \\ \mathbf{A}_{\mathcal{A}} \mathbf{M}_{\mathrm{v}}^{-1} \mathbf{A}_{\mathcal{S}}^{\mathrm{T}} & \mathbf{A}_{\mathcal{A}} \mathbf{M}_{\mathrm{v}}^{-1} \mathbf{A}_{\mathcal{A}}^{\mathrm{T}} \end{bmatrix} \tag{12}$$

It can also be shown that for a specified sub-space $\mathcal{S}$, the complementary sub-space and its Jacobian $\mathbf{A}_{\mathcal{A}}$ are not unique and it is always possible to select $\mathcal{A}$ in such a way that the off-diagonal terms in $\mathbf{M}_{\mathrm{w}}^{-1}$ vanish:

$$\mathbf{A}_{\mathcal{S}} \mathbf{M}_{\mathrm{v}}^{-1} \mathbf{A}_{\mathcal{A}}^{\mathrm{T}} = \mathbf{0}, \qquad \mathbf{A}_{\mathcal{A}} \mathbf{M}_{\mathrm{v}}^{-1} \mathbf{A}_{\mathcal{S}}^{\mathrm{T}} = \mathbf{0} \tag{13}$$

In this case, the two sub-spaces are orthogonal to each other (mass orthogonality), i.e. $\langle \mathbf{w}_{\mathcal{A}_m}, \mathbf{w}_{\mathcal{S}_n} \rangle = \delta_{mn}$, which enables us to decouple the system equation of motion. For a sub-space $\mathcal{S}$ and its orthogonal complement space $\mathcal{A}$, the dynamic equations can be transformed into [12]

$$\begin{bmatrix} \left(\mathbf{A}_{\mathcal{S}} \mathbf{M}_{\mathrm{v}}^{-1} \mathbf{A}_{\mathcal{S}}^{\mathrm{T}}\right)^{-1} & \mathbf{0} \\ \mathbf{0} & \left(\mathbf{A}_{\mathcal{A}} \mathbf{M}_{\mathrm{v}}^{-1} \mathbf{A}_{\mathcal{A}}^{\mathrm{T}}\right)^{-1} \end{bmatrix} \begin{bmatrix} \dot{\mathbf{w}}_{\mathcal{S}} \\ \dot{\mathbf{w}}_{\mathcal{A}} \end{bmatrix} + \begin{bmatrix} \mathbf{z}_{\mathcal{S}} \\ \mathbf{z}_{\mathcal{A}} \end{bmatrix} = \begin{bmatrix} \boldsymbol{\tau}_{\mathcal{S}} \\ \boldsymbol{\tau}_{\mathcal{A}} \end{bmatrix} + \begin{bmatrix} \boldsymbol{\lambda}_{\mathcal{S}} \\ \mathbf{0} \end{bmatrix} \tag{14}$$

where

$$\mathbf{z}_{\mathcal{S}} = \left(\mathbf{A}_{\mathcal{S}} \mathbf{M}_{\mathrm{v}}^{-1} \mathbf{A}_{\mathcal{S}}^{\mathrm{T}}\right)^{-1} \mathbf{A}_{\mathcal{S}} \mathbf{M}_{\mathrm{v}}^{-1} \mathbf{c} - \left(\mathbf{A}_{\mathcal{S}} \mathbf{M}_{\mathrm{v}}^{-1} \mathbf{A}_{\mathcal{S}}^{\mathrm{T}}\right)^{-1} \dot{\mathbf{A}}_{\mathcal{S}} \mathbf{v}$$

$$\mathbf{z}_{\mathcal{A}} = \left(\mathbf{A}_{\mathcal{A}} \mathbf{M}_{\mathrm{v}}^{-1} \mathbf{A}_{\mathcal{A}}^{\mathrm{T}}\right)^{-1} \mathbf{A}_{\mathcal{A}} \mathbf{M}_{\mathrm{v}}^{-1} \mathbf{c} - \left(\mathbf{A}_{\mathcal{A}} \mathbf{M}_{\mathrm{v}}^{-1} \mathbf{A}_{\mathcal{A}}^{\mathrm{T}}\right)^{-1} \dot{\mathbf{A}}_{\mathcal{A}} \mathbf{v}$$

are the decoupled Coriolis and centrifugal terms, and the generalized force terms can be given by

$$\boldsymbol{\tau}_{\mathcal{S}} = \left(\mathbf{A}_{\mathcal{S}}\mathbf{M}_{\mathrm{v}}^{-1}\mathbf{A}_{\mathcal{S}}^{\mathrm{T}}\right)^{-1}\mathbf{A}_{\mathcal{S}}\mathbf{M}_{\mathrm{v}}^{-1}\mathbf{f}$$

$$\boldsymbol{\tau}_{\mathcal{A}} = \left(\mathbf{A}_{\mathcal{A}}\mathbf{M}_{\mathrm{v}}^{-1}\mathbf{A}_{\mathcal{A}}^{\mathrm{T}}\right)^{-1}\mathbf{A}_{\mathcal{A}}\mathbf{M}_{\mathrm{v}}^{-1}\mathbf{f}$$

where $\mathbf{f}$ is the generalized force array of all other forces. Using such model order reduction is not limited to dynamic systems and it can also be used in other areas such as elastostatic or modal analysis as well [13].

B. Smooth and Non-Smooth Reduced Interface Models

In a co-simulation setup, we are interested in the sub-space of the motion associated with the *interface* of the subsystem since it only interacts with the rest of the system through its interface. Hence, if we select $\mathcal{S}$ to be the interface subspace i, according to (10) and the first row in (14), the dynamics associated with the interface subspace is explicitly factored out as

$$\left(\mathbf{A}_{\mathrm{i}}\mathbf{M}^{-1}\mathbf{A}_{\mathrm{i}}^{\mathrm{T}}\right)^{-1}\dot{\mathbf{w}}_{\mathrm{i}} + \underbrace{\left(\mathbf{A}_{\mathrm{i}}\mathbf{M}^{-1}\mathbf{A}_{\mathrm{i}}^{\mathrm{T}}\right)^{-1}\left(\mathbf{A}_{\mathrm{i}}\mathbf{M}^{-1}\mathbf{c} - \dot{\mathbf{A}}_{\mathrm{i}}\mathbf{v}\right)}_{\mathbf{z}_{\mathrm{i}}}$$

$$= \underbrace{\left(\mathbf{A}_{\mathrm{i}}\mathbf{M}^{-1}\mathbf{A}_{\mathrm{i}}^{\mathrm{T}}\right)^{-1}\left[\mathbf{A}_{\mathrm{i}}\mathbf{M}^{-1}(\mathbf{f}_{\mathrm{o}}+\mathbf{A}_{\alpha}^{\mathrm{T}}\boldsymbol{\lambda}_{\alpha}+\mathbf{A}_{\mathrm{t}}^{\mathrm{T}}\boldsymbol{\lambda}_{\mathrm{t}}+\mathbf{A}_{\mathrm{p}}^{\mathrm{T}}\boldsymbol{\lambda}_{\mathrm{p}})\right]}_{\boldsymbol{\tau}_{\mathrm{i}}} + \boldsymbol{\lambda}_{\mathrm{i}} \tag{15}$$

Note that $\boldsymbol{\lambda}_{\mathrm{t}}$ is a known value according to the definition of tight constraints. However, $\boldsymbol{\lambda}_{\alpha}$ and $\boldsymbol{\lambda}_{\mathrm{p}}$ are yet unknown and need to be determined. Now, if we select $\mathcal{S}$ to be the subspace associated with the active constraints α, according to (14), the dynamics associated with the constrained motion will be factored out and $\boldsymbol{\lambda}_{\alpha}$ will be calculated as

$$\boldsymbol{\lambda}_{\alpha} = \left(\mathbf{A}_{\alpha}\mathbf{M}^{-1}\mathbf{A}_{\alpha}^{\mathrm{T}}\right)^{-1}\left[\dot{\mathbf{w}}_{\alpha} - \mathbf{A}_{\alpha}\mathbf{M}^{-1}\left(\mathbf{f}_{\mathrm{o}} - \mathbf{c} + \mathbf{A}_{\mathrm{t}}^{\mathrm{T}}\boldsymbol{\lambda}_{\mathrm{t}}\right.\right.$$
$$\left.\left.+\mathbf{A}_{\alpha}^{\mathrm{T}}\boldsymbol{\lambda}_{\alpha} + \mathbf{A}_{\mathrm{p}}^{\mathrm{T}}\boldsymbol{\lambda}_{\mathrm{p}}\right) - \dot{\mathbf{A}}_{\alpha}\mathbf{v}\right] \tag{16}$$

where $\dot{\mathbf{w}}_{\alpha}$ is known and often zero. Here, we also assume that $\dot{\mathbf{w}}_{\alpha} = \mathbf{0}$. Substituting $\boldsymbol{\lambda}_{\alpha}$ from (16) into (15) will give

$$\mathbf{M}_{\mathrm{eff}}\dot{\mathbf{w}}_{\mathrm{i}} = \boldsymbol{\lambda}_{\mathrm{i}} + \mathbf{f}_{\mathrm{eff}} + \mathbf{M}_{\mathrm{eff}}\mathbf{H}_{\mathrm{ip}}\boldsymbol{\lambda}_{\mathrm{p}} \tag{17}$$

where

$$\mathbf{M}_{\mathrm{eff}} = \left[\mathbf{A}_{\mathrm{i}}(\mathbf{I}-\mathbf{P}_{\alpha})\mathbf{M}^{-1}\mathbf{A}_{\mathrm{i}}^{\mathrm{T}}\right]^{-1} \tag{18}$$

is the interface *effective mass*, and the *effective force* term can be given by

$$\mathbf{f}_{\mathrm{eff}} = \mathbf{M}_{\mathrm{eff}}\left[\mathbf{A}_{\mathrm{i}}(\mathbf{I}-\mathbf{P}_{\alpha})\mathbf{M}^{-1}\left(\mathbf{f}_{\mathrm{o}} - \mathbf{c} + \mathbf{A}_{\mathrm{t}}^{\mathrm{T}}\boldsymbol{\lambda}_{\mathrm{t}}\right)\right.$$
$$\left.+\left(\dot{\mathbf{A}}_{\mathrm{i}} - \mathbf{A}_{\mathrm{i}}\mathbf{M}^{-1}\mathbf{A}_{\alpha}^{\mathrm{T}}(\mathbf{A}_{\alpha}\mathbf{M}^{-1}\mathbf{A}_{\alpha}^{\mathrm{T}})^{-1}\dot{\mathbf{A}}_{\alpha}\right)\mathbf{v}\right]$$

Moreover, $\mathbf{H}_{\mathrm{ip}} = \mathbf{A}_{\mathrm{i}}(\mathbf{I}-\mathbf{P}_{\alpha})\mathbf{M}^{-1}\mathbf{A}_{\mathrm{p}}^{\mathrm{T}}$ is a generalized inverse mass matrix and, $\mathbf{P}_{\alpha} = \mathbf{M}^{-1}\mathbf{A}_{\alpha}^{\mathrm{T}}(\mathbf{A}_{\alpha}\mathbf{M}^{-1}\mathbf{A}_{\alpha}^{\mathrm{T}})^{-1}\mathbf{A}_{\alpha}$ is projector matrix.

If no potential contacts are considered at the first place, i.e. $\boldsymbol{\lambda}_{\mathrm{p}} = \mathbf{0}$, then (17) describes the dynamics of *smooth-RIM* that represents a reduced order model subjected only to bilateral constraints (assuming that state of the contacts will not change). This is also the formulation used in [5]. However, we can extend this further to include the complementarity of the potential contacts in the formulation as well. To this end, we employ (14) once more and expand the subspace $\mathcal{S}$ using potential constraint velocity $\mathbf{w}_{\mathrm{p}}$ which results in

$$\begin{cases} \dot{\mathbf{w}}_{\mathrm{p}} = \mathbf{H}_{\mathrm{pi}}\boldsymbol{\lambda}_{\mathrm{i}} + \mathbf{H}_{\mathrm{pp}}\boldsymbol{\lambda}_{\mathrm{p}} + \mathbf{b}_{\mathrm{p}} \\ \mathbf{0} \le \dot{\mathbf{w}}_{\mathrm{p}} \perp \boldsymbol{\lambda}_{\mathrm{p}} \ge \mathbf{0} \end{cases} \tag{19}$$

where

$$\mathbf{H}_{\mathrm{pi}} = \mathbf{A}_{\mathrm{p}}(\mathbf{I}-\mathbf{P}_{\alpha})\mathbf{M}^{-1}\mathbf{A}_{\mathrm{i}}^{\mathrm{T}}, \quad \mathbf{H}_{\mathrm{pp}} = \mathbf{A}_{\mathrm{p}}(\mathbf{I}-\mathbf{P}_{\alpha})\mathbf{M}^{-1}\mathbf{A}_{\mathrm{p}}^{\mathrm{T}}$$

are the generalized inverse mass matrices and

$$\mathbf{b}_{\mathrm{p}} = \mathbf{A}_{\mathrm{p}}(\mathbf{I}-\mathbf{P}_{\alpha})\mathbf{M}^{-1}\left(\mathbf{f}_{\mathrm{o}} - \mathbf{c} + \mathbf{A}_{\mathrm{t}}^{\mathrm{T}}\boldsymbol{\lambda}_{\mathrm{t}}\right)$$
$$+\left(\dot{\mathbf{A}}_{\mathrm{p}} - \mathbf{A}_{\mathrm{p}}\mathbf{M}^{-1}\mathbf{A}_{\alpha}^{\mathrm{T}}(\mathbf{A}_{\alpha}\mathbf{M}^{-1}\mathbf{A}_{\alpha}^{\mathrm{T}})^{-1}\dot{\mathbf{A}}_{\alpha}\right)\mathbf{v}$$

is the remaining nonlinear generalized acceleration terms. Equations (17) and (19) together form the *non-smooth-RIM* formulation that would allow for contact state transition also inside the macro time step:

$$\begin{cases} \begin{bmatrix} \mathbf{M}_{\mathrm{eff}} & -\mathbf{1} & -\mathbf{M}_{\mathrm{eff}}\mathbf{H}_{\mathrm{ip}} \\ \mathbf{0} & \mathbf{H}_{\mathrm{pi}} & \mathbf{H}_{\mathrm{pp}} \end{bmatrix} \begin{bmatrix} \dot{\mathbf{w}}_{\mathrm{i}} \\ \boldsymbol{\lambda}_{\mathrm{i}} \\ \boldsymbol{\lambda}_{\mathrm{p}} \end{bmatrix} + \begin{bmatrix} -\mathbf{f}_{\mathrm{eff}} \\ \mathbf{b}_{\mathrm{p}} \end{bmatrix} = \begin{bmatrix} \mathbf{0} \\ \dot{\mathbf{w}}_{\mathrm{p}} \end{bmatrix} \\ \mathbf{0} \le \dot{\mathbf{w}}_{\mathrm{p}} \perp \boldsymbol{\lambda}_{\mathrm{p}} \ge \mathbf{0} \end{cases} \tag{20}$$

The non-smooth-RIM formulation above will be transferred to the co-simulation manager and will be solved with their dynamic equations as a coupled equation during the macro time step.

IV. Numerical Solution

The non-smooth system dynamics can also be formulated at the impulse–momentum level. To this end, the dynamic equations are discretized in time and the velocity at the next time step $\mathbf{w}^{+} = \mathbf{w}(t_{\mathrm{k}} + h)$ can be approximated by first-order Taylor series expansion at t_{k} as

$$\mathbf{w}^{+} = \mathbf{w} + \frac{\mathrm{d}\mathbf{w}}{\mathrm{d}t}h + O(h^2) \tag{21}$$

where $\mathbf{w}$ is the known velocity at time t_{k} and h is the time step. By neglecting higher-order terms, such a time discretization is equivalent to first-order semi-implicit Euler integrator. Thus, the non-smooth-RIM formulation in (20) can be written as

$$\begin{cases} \begin{bmatrix} \mathbf{M}_{\mathrm{eff}} & -\mathbf{1} & -\mathbf{M}_{\mathrm{eff}}\mathbf{H}_{\mathrm{ip}} \\ \mathbf{0} & \mathbf{H}_{\mathrm{pi}} & \mathbf{H}_{\mathrm{pp}} \end{bmatrix} \begin{bmatrix} \mathbf{w}_{\mathrm{i}}^{+} \\ h\boldsymbol{\lambda}_{\mathrm{i}}^{+} \\ h\boldsymbol{\lambda}_{\mathrm{p}}^{+} \end{bmatrix} + \begin{bmatrix} -\mathbf{M}_{\mathrm{eff}}\mathbf{w}_{\mathrm{i}} - h\mathbf{f}_{\mathrm{eff}} \\ \mathbf{w}_{\mathrm{p}} + h\mathbf{b}_{\mathrm{p}} \end{bmatrix} = \begin{bmatrix} \mathbf{0} \\ \mathbf{w}_{\mathrm{p}}^{+} \end{bmatrix} \\ \mathbf{0} \le \mathbf{w}_{\mathrm{p}}^{+} \perp \boldsymbol{\lambda}_{\mathrm{p}}^{+} \ge \mathbf{0} \end{cases} \tag{22}$$

A. Constraint Regularization

Constraint redundancy occurs when two or more constraints become dependent on each other, i.e., limit the same constrained motion degrees of freedom. This is a common challenge in models with multiple contact interactions. A redundant system is an indeterminate problem where the rows of the constraint Jacobian are not independent and the matrix does not have a full row rank. As a result the individual constraint reactions cannot be determined uniquely considering the rigid body assumption alone. In such cases, constraint regularization (relaxation) can be used where additional information about the structural properties

of the system is added to the model in the form of compliance at the contact points. This "relaxes" the constraints in the model and the constraint forces can then be expressed with discretized constitutive relations such as

$$\boldsymbol{\lambda}_{\mathrm{c}}^{+} = -\mathbf{K}\boldsymbol{\Phi}_{\mathrm{c}}^{+} - \mathbf{D}\mathbf{w}_{\mathrm{c}}^{+} \tag{23}$$

where $\mathbf{K}$ and $\mathbf{D}$ are $m_{\mathrm{c}} \times m_{\mathrm{c}}$ diagonal stiffness and damping matrices. Then, $\boldsymbol{\Phi}_{\mathrm{c}}^{+}$ and $\mathbf{w}_{\mathrm{c}}^{+}$ can be approximated using finite differences to form a new representation for the constraint equations as

$$\mathbf{w}_{\mathrm{c}}^{+} = \mathbf{A}_{\mathrm{c}}\mathbf{v}^{+} + h\dot{\mathbf{A}}_{\mathrm{c}}\mathbf{v} + \boldsymbol{\Omega}_{\mathrm{c}}(h\boldsymbol{\lambda}_{\mathrm{c}}^{+}) + \boldsymbol{\Gamma}_{\mathrm{c}}(h^{-1}\boldsymbol{\Phi}_{\mathrm{c}}) \tag{24}$$

where $\boldsymbol{\Omega}_{\mathrm{c}} = (\mathbf{K}h^2 + \mathbf{D}h)^{-1}$ and $\boldsymbol{\Gamma}_{\mathrm{c}} = (\mathbf{1} + \mathbf{D}(\mathbf{K}h)^{-1})^{-1}$ are constant, positive-definite matrices containing the regularization terms. Subsequently, the regularized version of the terms in (17) and (22) can be written as

$$\begin{aligned}
\mathbf{f}_{\mathrm{eff}} &= \mathbf{M}_{\mathrm{eff}}\big[\mathbf{A}_{\mathrm{i}}(\mathbf{I}-\mathbf{P}_{\alpha})\mathbf{M}^{-1}\left(\mathbf{f}_{\mathrm{o}} - \mathbf{c} + \mathbf{A}_{\mathrm{t}}^{\mathrm{T}}\boldsymbol{\lambda}_{\mathrm{t}}\right) - h^{-1}\boldsymbol{\Pi}_{\mathrm{i}} \\
&\quad + (\dot{\mathbf{A}}_{\mathrm{i}} - \mathbf{A}_{\mathrm{i}}\mathbf{M}^{-1}\mathbf{A}_{\alpha}^{\mathrm{T}}(\mathbf{A}_{\alpha}\mathbf{M}^{-1}\mathbf{A}_{\alpha}^{\mathrm{T}} + \boldsymbol{\Omega}_{\alpha})^{-1}\dot{\mathbf{A}}_{\alpha})\mathbf{v}\big] \\
\mathbf{b}_{\mathrm{p}} &= \mathbf{A}_{\mathrm{p}}(\mathbf{I}-\mathbf{P}_{\alpha})\mathbf{M}^{-1}\left(\mathbf{f}_{\mathrm{o}} - \mathbf{c} + \mathbf{A}_{\mathrm{t}}^{\mathrm{T}}\boldsymbol{\lambda}_{\mathrm{t}}\right) - h^{-1}\boldsymbol{\Pi}_{\mathrm{p}} \\
&\quad + (\dot{\mathbf{A}}_{\mathrm{p}} - \mathbf{A}_{\mathrm{p}}\mathbf{M}^{-1}\mathbf{A}_{\alpha}^{\mathrm{T}}(\mathbf{A}_{\alpha}\mathbf{M}^{-1}\mathbf{A}_{\alpha}^{\mathrm{T}} + \boldsymbol{\Omega}_{\alpha})^{-1}\dot{\mathbf{A}}_{\alpha})\mathbf{v} \\
\mathbf{H}_{\mathrm{pp}} &= \mathbf{A}_{\mathrm{p}}(\mathbf{I}-\mathbf{P}_{\alpha})\mathbf{M}^{-1}\mathbf{A}_{\mathrm{p}}^{\mathrm{T}} + \boldsymbol{\Omega}_{\mathrm{p}} \\
\boldsymbol{\Pi}_{\mathrm{i}} &= \mathbf{A}_{\mathrm{i}}\mathbf{M}^{-1}\mathbf{A}_{\alpha}^{\mathrm{T}}\left(\mathbf{A}_{\alpha}\mathbf{M}^{-1}\mathbf{A}_{\alpha}^{\mathrm{T}} + \boldsymbol{\Omega}_{\alpha}\right)^{-1}\boldsymbol{\Gamma}_{\alpha}h^{-1}\boldsymbol{\Phi}_{\alpha} \\
\boldsymbol{\Pi}_{\mathrm{p}} &= \mathbf{A}_{\mathrm{p}}\mathbf{M}^{-1}\mathbf{A}_{\alpha}^{\mathrm{T}}\left(\mathbf{A}_{\alpha}\mathbf{M}^{-1}\mathbf{A}_{\alpha}^{\mathrm{T}} + \boldsymbol{\Omega}_{\alpha}\right)^{-1}\boldsymbol{\Gamma}_{\alpha}h^{-1}\boldsymbol{\Phi}_{\alpha} \\
&\quad + \boldsymbol{\Gamma}_{\mathrm{p}}h^{-1}\boldsymbol{\Phi}_{\mathrm{p}} \\
\mathbf{P}_{\alpha} &= \mathbf{M}^{-1}\mathbf{A}_{\alpha}^{\mathrm{T}}(\mathbf{A}_{\alpha}\mathbf{M}^{-1}\mathbf{A}_{\alpha}^{\mathrm{T}} + \boldsymbol{\Omega}_{\alpha})^{-1}\mathbf{A}_{\alpha}
\end{aligned} \tag{25}$$

V. Case Study

In this section, a co-simulation example is presented and analyzed for a robotic contact task. The multibody system being considered is a rigid 7-DoF robotic arm performing contact tasks and it is shown in Fig. 2. Here, the multibody system is divided into two subsystems; S1: the end-effector (EE), the payload and the environment and, S2: the remainder of the articulated arm. It is worth to note that all unilateral interactions occur in subsystem S1. All the links of the robot are modelled as uniform beams. The dimension and mass of each body of the robot are provided in Table I.

By such division, the motion of the EE in subsystem S1 can be described using 6 velocities and 7 coordinates (3 translational and 4 rotational coordinates), while the dynamics associated with the articulated arm S2 are expressed with minimal coordinates, i.e., the 7 joint coordinates and their rates. Subsystems S1 and S2 are connected at the cross section between the end-effector and the articulated arm as shown in Fig. 3. Therefore, the interface has 6 degrees of freedom and the reduced interface model of each subsystem will have 6 degrees of freedom. This will result in 6×6 and 6×1 effective mass and force matrices.

The time stepping frequency of the co-simulation is set for interactive rates, i.e., 60 Hz (resulting in $1/60$ s macro time step) while each subsystem will be solved with the reduced model of the other subsystem with the frequency of 600 Hz. To assess the obtained results, a monolithic solution of the entire system is

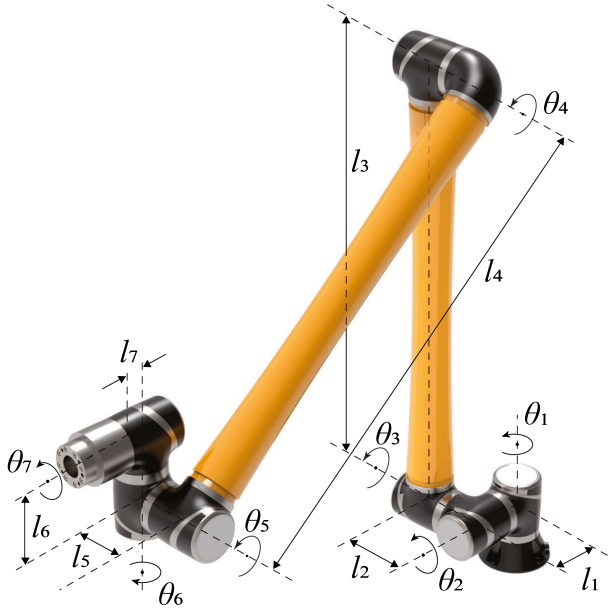

Fig. 2. 7-DoF robotic manipulator used as the case study.

TABLE I
Mechanical Parameters of the Case Study System

Link	Dimension	Mass
1	$l_1 = 0.64$ m	$m_1 = 121.2$ kg
2	$l_2 = 0.50$ m	$m_2 = 96.2$ kg
3	$l_3 = 6.85$ m	$m_3 = 1307.3$ kg
4	$l_4 = 6.85$ m	$m_4 = 1307.3$ kg
5	$l_5 = 0.50$ m	$m_5 = 96.2$ kg
6	$l_6 = 0.64$ m	$m_6 = 121.2$ kg
7	$l_7 = 0.38$ m	$m_7 = 72.5$ kg
End-effector	N/A	$m_{\mathrm{EE}} = 50$ kg
Payload (Box)	$4 \times 2 \times 1$ m	$m_{\mathrm{PL}} = 20$ kg

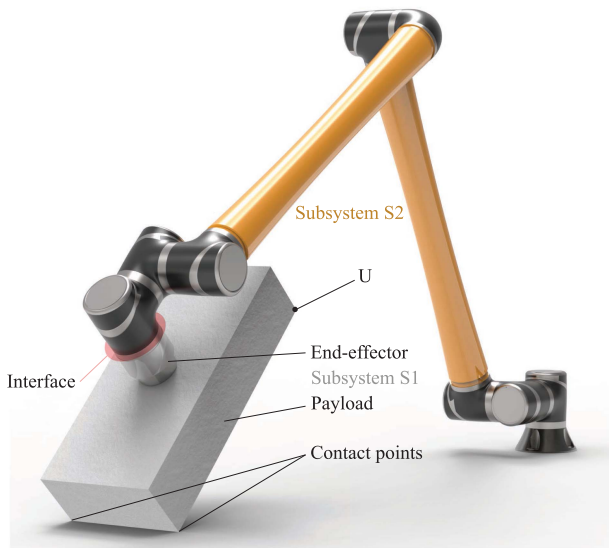

Fig. 3. Two subsystems of the co-simulation case study.

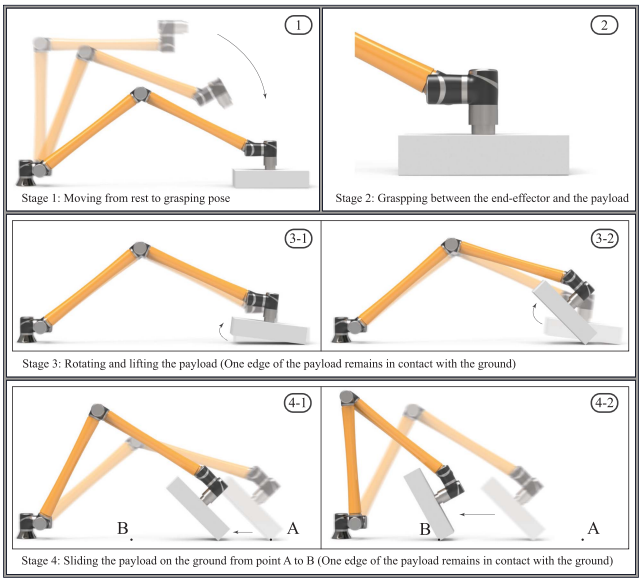

Fig. 4. Manoeuvre of the robot obtained by monolithic solution and also, the non-smooth RIM co-simulation.

also carried out with the integration frequency of 60 Hz for each task as the reference solution. The co-simulation implementation was done using MATLAB R2022b software.

A. Robot Capturing Task

In order to show the differences between the smooth and non-smooth RIMs, a manoeuvre has been designed for the robotic arm which consists in four stages in a total simulation time of 12 seconds (see Fig. 4). First, the robot starts from a resting position and moves toward a boxed shape payload resting on the ground in 4 seconds. Once the EE reaches the payload and as the second stage of the motion, a gripper attached to the EE is used to fully capture the payload fixture in half a second. The capturing will remove all 6 degrees of freedom of relative motion between the EE and the payload. At the third stage of the manoeuvre, the payload is lifted and rotated simultaneously so that one edge of the box remains in contact with the ground while it is rotated 45 degrees. The simulation time for this stage is 3.5 seconds. During the third stage of the movement, two points of the payload are in contact with the ground. As the final stage, the robot slides the payload toward itself for 4 seconds while the box edge and its corresponding two points remain in contact with the ground. This stage is also shown in Fig. 3.

The torques required to actuate the joints for such a manoeuvre are generated through an inverse dynamic analysis of the model using the monolithic formulation. Once the time history of the torques are captured, it will be used as the input for all the simulations presented in following sections.

As shown in Fig. 4, the described manoeuvre is designed in such way that the payload will get in contact with the ground continuously at two points. Treating these contacts as active or potential, will cause different outcomes which will be discussed in the next section.

VI. Results and Discussion

A. Smooth RIM vs Non-Smooth RIM

In the first part of the designed trajectory where the EE moves toward the payload resting on the ground, both smooth and non-smooth RIMs will give the same results as the reference solution. The difference starts to show when the EE captures the payload. We recall that, the first subsystem S1 includes the EE, payload and the environment (ground). The EE and the payload (box) are considered as rigid bodies and hence, each has 6 DoF resulting in a possible total of 12 DoF for subsystem S1 without considering any constraints. When the payload capture occurs, the 6 DoF relative motion between the EE and the payload will be constrained, which leaves only 6 DoF for the subsystem S1. However, in the third stage of the manoeuvre (see Fig. 4) where the robot tries to lift and rotate the payload, two vertices of the box are constantly touching the ground. Using the non-smooth RIM, these two points are treated as potential contact points and their effect on the robot motion is taken into account by determining $\boldsymbol{\lambda}_{\mathrm{p}}$ through solving the Mixed-LCP in (20). Thus, the set of active constraints includes the 6 bilateral constraints between EE and the payload resulting in a 6×6 positive-definite effective mass $\mathbf{M}_{\mathrm{eff}}$ which is fully representative of the 6 DoF interface.

On the other side, using the smooth RIM approach, no potential contacts are considered. Therefore, at the same posture at stage four, the two contact points are considered as bilateral constraints (during the macro time step) and are grouped as active constraints. This will give 8 active constraints (6 for the capturing and 2 contact points) that are redundant and the projector $\mathbf{I} - \mathbf{P}_{\alpha}$ in (18) becomes a 12×12 matrix which only contains 4 independent rows. The projection in this case produces an ill-conditioned 6×6 effective mass matrix with rank 4, which cannot be representative of a 6 DoF interface. This is why such a modelling using smooth-RIM is invalid. It should be noted that the smooth RIM formulation is not really usable from the moment the box is captured by the EE ($t \simeq 4$s). However, due to MATLAB's built-in features, the simulation continues with warnings. The motion of the system using the smooth RIM co-simulation is shown in Fig. 5. It can be seen that, the obtained motion from the simulation is different from the expected reference motion. The difference stems from the moment that the robot is trying to rotate and lift the box off the ground but due to the constraint redundancy and rank deficiency of the effective mass matrix, the simulation continues inaccurately and the box suddenly jumps off the ground.

To compare the methods quantitatively, the position and velocity of one the vertices of the payload marked as U (see Fig. 3) are captured during the simulation. Figs. 6 and 7 show the three components of position and velocity of U, respectively, obtained through each method. Both figures indicate that there is a visual correlation between the results obtained through non-smooth RIM and the reference solution. However, to measure the correlation better, the absolute error of each position and velocity component with respect to the reference is computed and depicted in Fig. 8. The maximum error values for position and velocity are 2.42 cm and 0.62 m/s for non-smooth

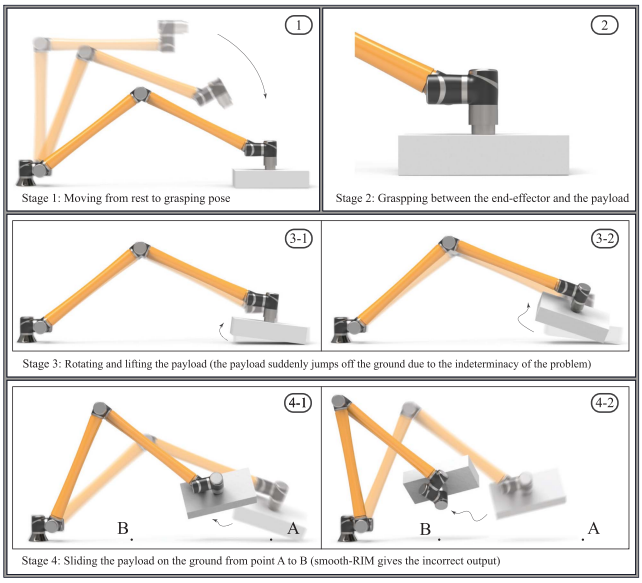

Fig. 5. Manoeuvre of the robot obtained by smooth-RIM co-simulation using the same inputs as the monolithic solution.

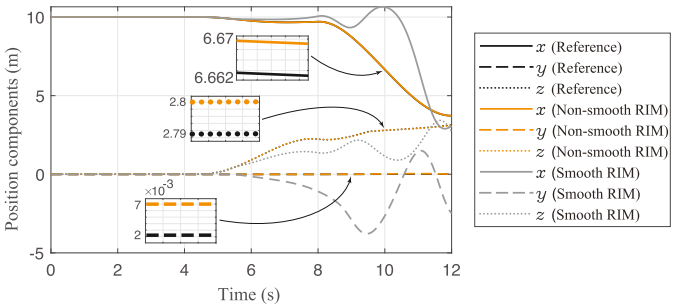

Fig. 6. Position components of point U on the payload obtained using monolithic solution (black), smooth RIM (blue) and, non-smooth RIM (red).

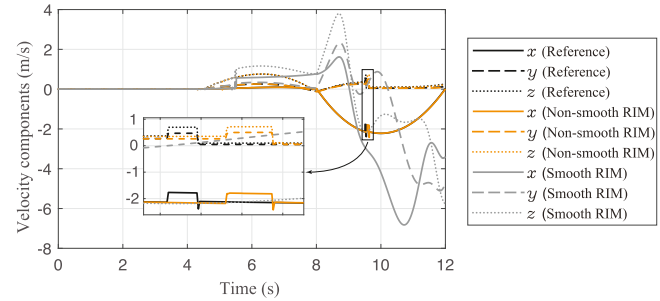

Fig. 7. Velocity components of point U on the payload obtained using monolithic solution (black), smooth RIM (blue) and, non-smooth RIM (red).

RIM while these values are significantly higher for the smooth RIM. It is worth mentioning that the error in the results obtained by the non-smooth RIM is due to a slight delay between the results. Since there are no feedback controllers, the contact attachment/detachments in the simulations are not occurring at the exact same time. Otherwise, the errors would have been even lower. Moreover, in the first 4 seconds of the simulation the box is resting on the ground and the position and the velocity of point U are constant in all methods. However, the difference between

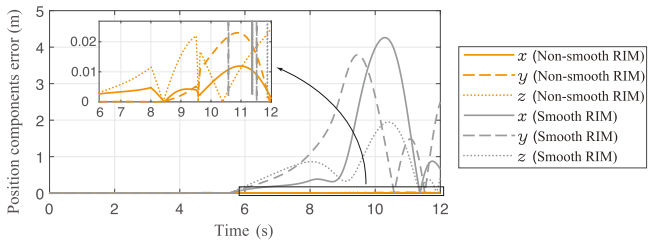

(a) Position components absolute errors

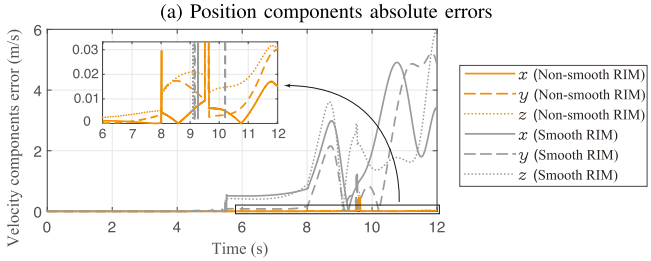

(b) Velocity components absolute errors

Fig. 8. Absolute errors of position and velocity components of point U obtained using smooth RIM and non-smooth RIM, compared to the reference solution.

the results starts to show from $t = 4.5\,\mathrm{s}$ where the third stage of the motion begins.

B. Constraint Regularization

It was seen that the smooth RIM can produce ill-conditioned effective mass matrix due to constraint redundancy. As was mentioned in Section IV-A, one way to tackle constraint redundancy is through regularization. This is not always a preferable choice as it changes the model by adding compliance to the interacting parts. In reality, perfect rigid body interaction does not exist and there is always a finite stiffness associated with each body. However, determining the stiffness and damping coefficients is not always straightforward.

To show this, here we regularized the unilateral interactions in the smooth-RIM based co-simulation using different stiffness and damping values. To compare the accuracy of the obtained results, a *root mean square* (RMS) of the absolute errors in position and velocity of point U is calculated. The RMS of an error associated with any variable y can be expressed as

$$\mathrm{RMS}(y - y_{\mathrm{ref}}) = \sqrt{\frac{1}{N}\sum_{k=1}^{N}\Big(y(t_k) - y_{\mathrm{ref}}(t_k)\Big)^2} \tag{26}$$

where y_{ref} is the reference solution, and N is the number of sampling data points.

The RMS of error in position and velocity magnitudes of point U as well as their components are shown in Fig. 9 for different values of regularization stiffness K. We also included damping to the model and in all cases, $D = K/(10^4\ s^{-1})$. In theory, increasing the contact stiffness should constantly decrease the error to the point that an infinite contact stiffness should deliver same results as the reference solution. But, numerically it is impossible to set K to infinity. By looking at $\mathbf{M}_{\mathrm{eff}}$ formulation and $\mathbf{P}_\alpha$ in (18) and (25), it can be said that there is an optimum value K_{opt} for regularization stiffness and increasing/decreasing further from that point will give more inaccurate results. For

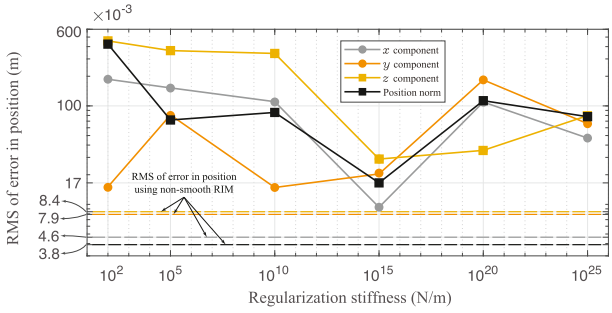

(a) RMS of error in position of point U.

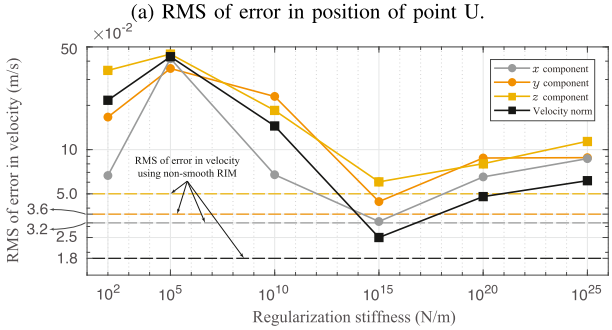

(b) RMS of error in velocity of point U.

Fig. 9. RMS of errors in position and velocity of point U with respect to the reference solution for different values of contact stiffness K, obtained using regularized smooth RIM co-simulation.

$K < K_{\text{opt}}$, the excessive compliance of the contact point will cause the results to stray away from the reference solution. Also, too large values of stiffness, $K > K_{\text{opt}}$, will force entities of the regularization term $\mathbf{\Omega}_\alpha$ to go to zero ($\mathbf{\Omega}_\alpha \to \mathbf{0}$) which in practice, removes the regularization term and delivers the same singular effective mass matrix as prior to the regularization.

Taking these into account, and looking at Fig. 9, it can be seen that increasing the contact stiffness up to $K = 10^{15}$ N/m will improve the RMS of errors. It is worth mentioning that although $K = 10^2$ N/m shows a lower error in velocity, large penetrations were observed between the box and the ground. The figure also shows that further increasing the contact stiffness from $K = 10^{15}$ N/m gives higher error values. During the simulations for cases $K = 10^{20}$ N/m and 10^{25} N/m, we were also encountered with matrix singularity warnings from MATLAB which was predictable. The same RMS of the errors for non-smooth RIM co-simulation are also depicted in Fig. 9 with dashed lines. It can be seen that the error values obtained from non-smooth RIM are always lower than their counterparts that are obtained based on the regularized smooth RIM.

VII. Conclusion

Two contact representation schemes were presented in this letter using a model-based co-simulation framework. In both approaches, a reduced model of the mechanical system is derived to represent the dynamic behaviours of the full model at the interface. The smooth RIM, assumes that the contact states will remain unchanged during the macro time step while, the non-smooth RIM, involves selecting potential contact points and determining their status through the solution of an LCP during the macro step. This accommodates contact detachments between the communication points, which can be important in certain situations. To illustrate this, we used the example of a robotic arm with a contact task, and found that the smooth RIM can be a bottleneck in this case, as it is not able to produces meaningful results. Smooth RIM can lead to over-constrained reduced models in certain cases and produce ill-conditioning. One common approach to addressing over-constrained systems is to regularize some of the constraints by introducing constitutive relations. However, this can change the system model and determining the proper stiffness and damping coefficients for such interactions is not straightforward. As our results show, using too low or high values can degrade the accuracy, and finding the appropriate values requires either a careful evaluation of the actual system or trial and error. In contrast, using the non-smooth RIM as an alternative to the smooth RIM allows the analyst to obtain meaningful results without altering the model of the system.

References

[1] B. Schweizer, D. Lu, and P. Li, "Co-simulation method for solver coupling with algebraic constraints incorporating relaxation techniques," *Multibody Syst. Dyn.*, vol. 36, no. 1, pp. 1–36, 2016.

[2] M. Arnold, *Numerical Methods for Simulation in Applied Dynamics*. Vienna, Austria: Springer, 2009.

[3] X. Dai, A. Raoofian, J. Kövecses, and M. Teichmann, "Model-based co-simulation of flexible mechanical systems with contacts using reduced interface models," *IEEE Robot. Automat. Lett.*, vol. 9, no. 1, pp. 239–246, Nov. 2023.

[4] O. Oberschelp and H. Vocking, "Multirate simulation of mechatronic systems," in *Proc. IEEE Int. Conf. Mechatronics*, 2004, pp. 404–409.

[5] A. Peiret, F. González, J. Kövecses, and M. Teichmann, "Co-simulation of multibody systems with contact using reduced interface models," *J. Comput. Nonlinear Dyn.*, vol. 15, no. 4, 2020, Art. no. 041001.

[6] A. Raoofian, A. Peiret, J. Kövecses, and M. Teichmann, "Non-smooth unilateral reduced models for co-simulation of mechanical systems," *Mechanism Mach. Theory*, vol. 173, 2022, Art. no. 104829.

[7] A. Peiret, F. González, J. Kövecses, and M. Teichmann, "Multibody system dynamics interface modelling for stable multirate co-simulation of multiphysics systems," *Mechanism Mach. Theory*, vol. 127, pp. 52–72, 2018.

[8] A. Peiret, F. González, J. Kövecses, M. Teichmann, and A. Enzenhoefer, "Model-based coupling for co-simulation of robotic contact tasks," *IEEE Robot. Automat. Lett.*, vol. 5, no. 4, pp. 5756–5763, Oct. 2020.

[9] V. Acary and B. Brogliato, *Numerical Methods for Nonsmooth Dynamical Systems: Applications in Mechanics and Electronics*. Berlin, Germany: Springer, 2008.

[10] F. Pfeiffer and C. Glocker, *Multibody Dynamics With Unilateral Contacts*, vol. 421. Berlin, Germany: Springer, 2000.

[11] J. C. Trinkle, J.-S. Pang, S. Sudarsky, and G. Lo, "On dynamic multi-rigid-body contact problems with coulomb friction," *ZAMM- J. Appl. Math. Mechanics/Zeitschrift für Angewandte Mathematik und Mechanik*, vol. 77, no. 4, pp. 267–279, 1997.

[12] J. Kövecses, "Dynamics of mechanical systems and the generalized free-body diagram—Part I: General formulation," *J. Appl. Mechanics*, vol. 75, no. 6, 2008, Art. no. 061012.

[13] A. Raoofian, A. Taghvaeipour, and A. Kamali, "Elastodynamic analysis of multibody systems and parametric mass matrix derivation," *Mechanics Based Des. Structures Mach.*, vol. 50, no. 10, pp. 3626–3648, 2020.